Journal of Neurochemistry

JOURNAL OF NEUROCHEMISTRY | 2011 | 117 | 554–564

doi: 10.1111/j.1471-4159.2011.07226.x

Acrolein induces myelin damage in mammalian spinal cord

Yunzhou Shi,*,[1] Wenjing Sun,†,[1] Jennifer J. McBride,† Ji-Xin Cheng*,‡ and Riyi Shi*,†

*Weldon School of Biomedical Engineering, Purdue University, West Lafayette, Indiana, USA

†Department of Chemistry, Purdue University, West Lafayette, Indiana, USA

‡Department of Basic Medical Sciences, Purdue University, West Lafayette, Indiana, USA

Abstract

Myelin damage can lead to the loss of axonal conduction and paralysis in multiple sclerosis and spinal cord injury. Here, we show that acrolein, a lipid peroxidation product, can cause significant myelin damage in isolated guinea pig spinal cord segments. Acrolein-mediated myelin damage is particularly conspicuous in the paranodal region in both a calcium dependent (nodal lengthening) and a calcium-independent manner (paranodal myelin splitting). In addition, paranodal protein complexes can dissociate with acrolein incubation. Degraded myelin basic protein is also detected at the paranodal region. Acrolein-induced exposure and redistribution of paranodal potassium channels and the resulting axonal conduction failure can be partially reversed by 4-AP, a potassium channel blocker. From this data, it is clear that acrolein is capable of inflicting myelin damage as well as axonal degeneration, and may represent an important factor in the pathogenesis in multiple sclerosis and spinal cord injury.

Keywords: axon, calcium, calpain, myelin, node, potassium channels.

J. Neurochem. (2011) **117**, 554–564.

Demyelination leads to varying degrees of axonal conduction impairment and debilitating functional deficits seen in diseases and trauma such as multiple sclerosis (MS) and spinal cord injury (SCI) (Blight 1985; Smith *et al.* 1999; Compston and Coles 2008). It is well established that inflammation plays a critical role in causing myelin damage in MS (Gold *et al.* 2006; Compston and Coles 2008). However, the mechanisms by which inflammation leads to demyelination remain to be established.

There is growing evidence that oxidative stress, which results at least in part from inflammation, plays a major role in the pathogenesis of MS (LeVine 1992; Smith *et al.* 1999; Jana and Pahan 2007; Gonsette 2008). There are numerous reports of increasing concentrations of reactive oxygen species and lipid peroxidation in both MS and SCI (Hall 1989; Povlishock and Kontos 1992; Calabrese *et al.* 1998; Koch *et al.* 2006). Furthermore, it has been reported that oxidative stress resulting from mitochondrial dysfunction plays a significant destructive role in demyelination that is independent of, or occurs prior to, inflammation (Smith *et al.* 1999). However, conventional strategies aiming to scavenge free radicals have not established any effective treatment that lessens neuronal function loss in either MS or SCI. Hence, further understanding of the mechanisms of oxidative stress and identification of particular targets for effective intervention are of great interest.

Recent evidence suggests that acrolein, a product of lipid peroxidation, may play a critical role in oxidative stress (Esterbauer *et al.* 1991; Adams and Klaidman 1993; Luo and Shi 2004). Aldehydes, such as acrolein and other related compounds have been shown to be present at increased concentrations following SCI (Luo *et al.* 2005b) and are significantly toxic to the nervous tissue (Lovell *et al.* 2000, 2001; Shi *et al.* 2002; Luo and Shi 2004, 2005). Acrolein is the strongest electrophile among the unsaturated aldehydes (Esterbauer *et al.* 1991). Acrolein formed *in vivo* is highly reactive with various biomolecules including phospholipids

Received November 15, 2010; revised manuscript received February 9, 2011; accepted February 21, 2011.

Address correspondence and reprint requests to Riyi Shi, Department of Basic Medical Sciences, Purdue University, 408 S. University Street, West Lafayette, IN 47907, USA. E-mail: riyi@purdue.edu; Ji-Xin Cheng, Weldon School of Biomedical Engineering, Department of Chemistry, Purdue University. West Lafayette, IN 47907, USA. E-mail: jcheng@purdue.edu

[1]These authors contributed equally to this study.

Abbreviations used: BSA, bovine serum albumin; CAP, compound action potential; Caspr, contactin associate protein; Caspr, contactin associate protein; EAE, experimental autoimmune encephalomyelitis; MBP, myelin basic protein; MS, multiple sclerosis; NFC2, pan anti-neurofascin; PBS, phosphate-buffered saline; SCI, spinal cord injury; TPEF, two photon excitation fluorescence; VGPC, voltage-gated potassium channels.

and proteins, two major components of the myelin sheath (Esterbauer *et al.* 1991; Kehrer and Biswal 2000). Acrolein, which persists for hours to days, also remains active in the body much longer than other, more commonly studied, reactive oxygen species (Ghilarducci and Tjeerdema 1995). Further, acrolein is also produced in greater concentrations (at least 40 times) than other alkenals such as 4-hydroxy-nonenal (Esterbauer *et al.* 1991). Therefore, acrolein may play a particularly damaging role in oxidative stress and myelin damage. To further support this notion, a recent report demonstrated a significantly increased of acrolein in the spinal cord of experimental autoimmune encephalomyelitis (EAE) mice, an animal model of multiple sclerosis (Leung *et al.* 2011). In addition, anti-acrolein treatment significantly improved behavioral performance and decreased myelin damage in spinal cord (Leung *et al.* 2011).

The purpose of this study was to investigate the effects of acrolein in demyelination using isolated guinea pig spinal cord ventral white matter, which consists of mostly myelinated axons. By coherent anti-stokes Raman scattering (CARS) imaging of myelin without labeling (Wang *et al.* 2005), we have found that acrolein was indeed capable of inducing significant myelin damage, particularly in the paranodal region. This finding suggests that acrolein plays a significant role in inflicting myelin damage and may serve as an effective target for therapeutic intervention in various diseases and trauma of nervous system.

Materials and methods

Animal surgery

The isolation of guinea pig spinal cords has been described previously (Shi and Blight 1996) (Shi and Whitebone 2006). Briefly, adult female guinea pigs (350–450 g) were anesthetized with an intramuscular injection of 80 mg/kg ketamine hydrochloride, 0.8 mg/kg acepromazine maleate, and 12 mg/kg xylazine. The animal was then perfused transcardially with cold (4°C) Krebs solution containing (in mM): NaCl 124, KCl 2, KH_2PO_4 1.2, $MgSO_4$ 1.3, $CaCl_2$ 2, dextrose 10, $NaHCO_3$ 26 and ascorbic acid 3, equilibrated with 95% O_2/5% CO_2. The vertebral column was then removed and the spinal cord was excised. The cord was first divided mid-sagitally into two strips of hemi-cord, and then ventral columns were gently dissected. The ventral white matter strips at a length of 40 mm were maintained in Krebs solution at 25°C bubbled with 95% O_2/5% CO_2 until the time of usage.

Electrophysiology

Compound action potentials (CAPs) were measured on the ventral columns placed in double sucrose gap recording apparatus as previously described (Shi and Blight 1996; Shi and Borgens 1999; Shi and Whitebone 2006). Briefly, the spinal cord strip was positioned in the chamber with central compartment continuously circulated with 37°C Krebs solution. The spinal cord strip was stimulated at one side, and compound action potential (CAP) was recorded at the opposite side of the strip. Every electrophysiological test was digitized in real time and captured to the computer for subsequent quantitative evaluation. All solutions used in the test were prepared fresh on the day of usage.

A typical 30-min period was given for the sample to stabilize after it was placed in the apparatus. Acrolein with (Sigma, St. Louis, MO, USA) was directly dissolved into ascorbic acid-free Krebs solution which was circulated through the central compartment at 37°C for at least 1 h. Acrolein incubation was followed by a wash period with regular Krebs solution. 4-AP (Sigma) dissolved in normal Krebs (100 μM) was then applied, followed by wash until the CAPs were stabilized.

CARS and immunofluorescence imaging

We used CARS to image myelin and two photon excitation fluorescence (TPEF) to image immunofluorescence signal simultaneously (Wang *et al.* 2005; Fu *et al.* 2007). The schematic diagram of the CARS has been shown previously (Wang *et al.* 2005). The pump and Stokes beams generated from two Ti:sapphire oscillators (Mira900, Coherent Inc., Santa Clara, CA, USA) with a beam width of 2.5 ps, ω_p-ω_s at 2840 cm^{-1}, were collinearly combined, passing through a Pockels' cell (Model 350–160, Conoptics, Danbury, CT, USA) directed into a confocal scanning microscope (Olympus Inc., Tokyo, Japan, FV300/IX70) equipped with a 60× water immersion objective (numerical aperture = 1.2, Olympus). Photomultiplier tubes (R3896, Hamamatsu, Japan) were used for CARS detection with two 600/65 nm bandpass filters (46–7332, Ealing Catalog Inc., Rocklin, CA, USA) and TPEF signal of oregon green 488 BAPTA-2 AM (Sigma) with a 520/40 filter (Ealing Catalog Inc.) simultaneously. The average pump and Stokes laser power at the sample were approximately 3.6 mw and 1.2 mw, respectively, with no observed photodamage. All the imaging experiments were carried out at room temperature (23°C). FluoView software (Olympus) was used to merge TPEF and CARS images. We used the antibody against degraded myelin basic protein (rabbit anti-degraded myelin basic protein AB5864, 1 : 1000, Chemicon, Temecula, CA, USA) to examine the damage induced by acrolein. In addition, rabbit raised anti-contactin associate protein (Caspr) and pan anti-neurofascin antibody (NFC2) (dilution ratio 1 : 100 for both, the monoclonal antibodies were developed by and obtained from the UC Davis/NIH NeuroMab Facility, supported by NIH grant U24NS050606 and maintained by the Department of Neurobiology, Physiology and Behavior, College of Biological Sciences, University of California, Davis, CA 95616) were used to examine the structure change of paranodal protein complex. Rabbit anti-Kv 1.2 (1 : 100, Alomone labs, Jerusalem, Israel) was used to label Kv 1.2 potassium channels. All the immunohistochemical procedures were carried out as described previously (Li and Stys 2000; Sasaki *et al.* 2006). In short, hemi-cord segments were first incubated in acrolein solution (200 μM) for 12 h at 25°C. The cord segments were then fixed in 4% paraformaldehyde solution for 24 h and followed with cryprotection (20% glycerol, 2% paraformaldehyde) at 4°C for 48 h. The samples were then cut into 50 μm sections by vibratome (OT-4000 Electron Microscope Sciences, Hatfield, PA, USA). Sections were then incubated in 0.5% Triton X-100 in phosphate-buffered saline (PBS) for 30 min, followed by PBS containing 1% bovine serum albumin (BSA) and 0.1% Triton X-100 for 1 h, and then washed in PBS for 1 h. Next, we incubated the sections in primary antibody diluted in PBS (containing 1% BSA and 0.1% Triton X-100 at 4°C)

overnight. After washing, the samples were then treated with the appropriate secondary antibody diluted in PBS (containing 1% BSA and 0.1% Triton X-100) for 2 h. FITC-goat anti-rabbit IgG (H + L) (1 : 100, Invitrogen, Carlsbad, CA, USA) was used as secondary antibody. We then washed the samples three times for a total of 30 min. Control groups were pre-incubated in ascorbic acid-free Krebs solution and went through the same process.

Statistics

Independent experiments using spinal cords from different guinea pigs were performed to determine the average values and standard error (SE), expressed in mean ± SE. ANOVA followed by *post-hoc* Tukey test was used for comparisons between multiple groups.

Results

Acrolein causes myelin retraction at nodes of Ranvier

To determine the effects of acrolein, we monitored the myelin sheath in isolated spinal tracts, both at nodes of Ranvier and internodal regions, using CARS microscopy. Figure 1 showed two representative nodes of Ranvier imaged from control tissue (Fig. 1a) and 12 h 200 μM acrolein treated tissue (Fig. 1b). When compared to healthy spinal cord (Fig. 1a), one notable change of the myelin in response to acrolein treatment was the lengthening of the node of Ranvier (Fig. 1b), expressed by the index of nodal length, calculated as the length of node (d_r) divided by the axon diameter (d_a) (Fig. 1c). Specifically, the length of node was measured by the longitudinal distance between the compact myelin loops on the two sides of the nodes (Fig. 1c). Quantitative analysis was carried out using two concentrations of acrolein (200 μM and 500 μM) to examine the prevalence of nodal retraction as well as the dose response. When treated with acrolein at 500 μM for 6 h, the average index of nodal length (d_r/d_a) was 1.43 ± 0.14 (n = 36) which was significantly higher than control group (0.56 ± 0.05, n = 44, $p < 0.01$). In the group where cord samples were treated with acrolein at 200 μM for 6 h, the average index of nodal length was 0.75 ± 0.05 (n = 47) which tended to be higher than controls, although it did not reach statistical significance ($p > 0.05$) (Fig. 1c). However, when treated for 12 h, acrolein at both 200 μM and 500 μM induced significant increase of the index of nodal length (1.87 ± 0.16, n = 79 and 2.95 ± 0.35, n = 41, respectively), compared to that of control (0.64 ± 0.07, n = 50, $p < 0.01$) (Fig. 1c). The difference was also significant between the 200 μM and 500 μM groups ($p < 0.01$) (Fig. 1c).

Acrolein induces myelin splitting at paranodal region

Normally, the membrane of terminal loops or the layers of the myelin lamella are tightly compacted together. In the acrolein treated tissues, however, we observed myelin splitting or loosening (loss of compaction) at the paranodal region (Fig. 2a and b). To quantify the myelin splitting, we

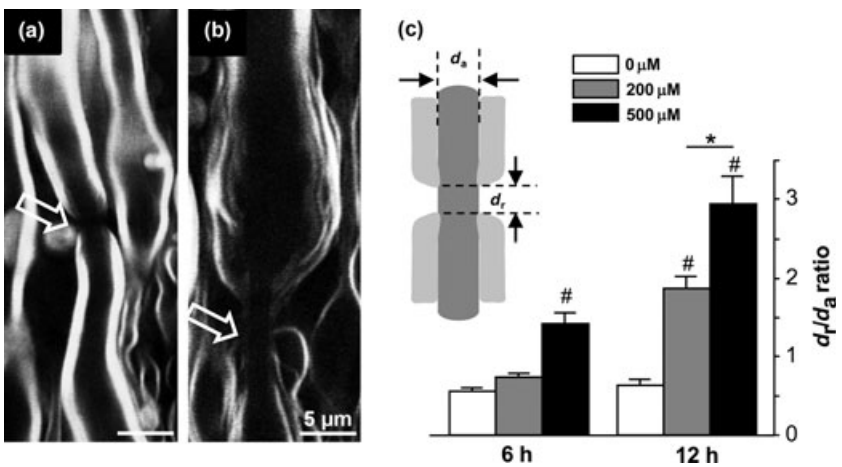

Fig. 1 CARS imaging of paranodal myelin retraction with acrolein incubation. (a–b) Representative CARS images show representative node of Ranvier from control sample (a) and myelin retraction at nodes of Ranvier (arrowhead) with 12 h acrolein incubation at 200 μM (b). (c) Schematics show quantitative measurement of individual axon diameter (d_a) and exposed nodal length (d_r) at the node of Ranvier. Three groups of spinal cord with five cords each were incubated with 0 μM, 200 μM, and 500 μM acrolein in oxygenated Krebs' solutions for up to 12 h. Images of 10–25 nodes of Ranvier were randomly collected in each sample at initial, 6 h and 12 h. The histogram of the index of nodal length (d_r/d_a) shows comparisons among all the experimental groups. At 6 h, 500 μM Acrolein incubation significantly increased the index of nodal length (d_r/d_a) from 0.56 ± 0.05 (n = 44) to 1.43 ± 0.14 (n = 36) ($p < 0.01$). 200 μM Acrolein incubation induced a higher index of nodal length of 0.75 ± 0.05 (n = 47) without reaching statistically significant level ($p > 0.05$). At 12 h, both 200 μM and 500 μM incubation significantly increased the index of nodal length (1.87 ± 0.16, n = 79 and 2.95 ± 0.35, n = 41 respectively, $p < 0.01$ for both). Also, the difference in index of nodal length between the two concentration groups was significant ($p < 0.01$, for both 6 h and 12 h). For all images, ω_p-ω_s was tuned to 2840 cm^{-1} for symmetric CH_2 stretch. Scale bar = 5 μm. #$p < 0.01$ compared to control. *$p < 0.05$.

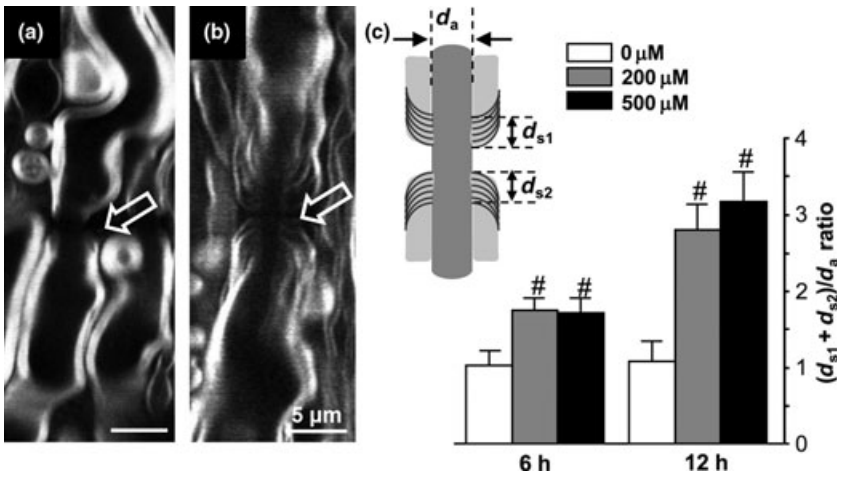

Fig. 2 CARS imaging of paranodal myelin splitting by acrolein. (a–b) Representative CARS images show representative control (a) and acrolein treatment induced myelin splitting at nodes of Ranvier (b). Acrolein at concentration of 200 μM was added for 12 h. (c) Schematics show quantitative measurement of individual axon diameter (d_a) and nodal splitting length (d_{s1}, d_{s2}). Both 200 μM and 500 μM treatment significantly increased the index of paranodal myelin [$(d_{s1} + d_{s2})/d_a$] (1.76 ± 0.16, $n = 47$, and 1.72 ± 0.21, $n = 36$, respectively) compared to the control group (1.02 ± 0.20, $n = 44$, $p < 0.01$) 6 h after treatment. There was no significant difference between the two concentration groups ($p > 0.05$). Twelve hours after treatment, both 200 μM and 500 μM induced further myelin splitting (2.79 ± 0.34, $n = 79$ and 3.16 ± 0.40, $n = 41$, respectively) compare to control (1.08 ± 0.25, $n = 50$, $p < 0.01$ for both). The original images used in quantification were the same images used Fig. 1. Scale bar = 5 μm. #$p < 0.01$ compared to control.

measured the length of uncompacted myelin along the longitudinal axis of the axon on both sides of the node (d_{s1} and d_{s2}, Fig. 2c) and the axonal diameter (d_a). We defined the index of paranodal myelin as $(d_{s1} + d_{s2})/d_a$ (Fig. 2c). Compared with the control healthy spinal cord (Fig. 2a), 12 h incubation of 200 μM acrolein noticeably disrupted the major dense lines of myelin sheath at paranodal region (Fig. 2b). Quantification was carried out by using acrolein at concentrations of 200 μM and 500 μM for 6 h or 12 h. At 6 h after treatment, acrolein at both 200 μM and 500 μM induced a significant increase in the index of paranodal myelin [$(d_{s1} + d_{s2})/d_a = 1.76 \pm 0.16$, $n = 47$, and $(d_{s1} + d_{s2})/d_a = 1.72 \pm 0.21$, $n = 36$, respectively] which were significantly different compared to the controls [$(d_{s1} + d_{s2})/d_a = 1.02 \pm 0.20$, $n = 44$, $p < 0.01$] (Fig. 2c). There was no significant difference between the two treatment groups (200 μM and 500 μM, 6 h, $p > 0.05$). The splitting tended to become more severe when treated with acrolein for 12 h. Specifically, acrolein at both 200 μM and 500 μM produced significantly higher indices of myelin splitting [$(d_{s1} + d_{s2})/d_a = 2.79 \pm 0.34$, $n = 79$ and $(d_{s1} + d_{s2})/d_a = 3.16 \pm 0.40$, $n = 41$, respectively] when compared to control [$(d_{s1} + d_{s2})/d_a = 1.08 \pm 0.25$, $n = 50$, $p < 0.01$] (Fig. 2c). There was no significant difference between the two treatment groups at 12 h (200 μM and 500 μM, $p > 0.05$). In summary, our results indicate that acrolein can produce significant myelin damage. In particular, acrolein induces myelin retraction in the paranodal region and increases the length of uncompacted myelin sheath at 200 μM or 500 μM when incubated for 6–12 h.

Myelin retraction is Ca^{2+} dependent while myelin splitting is not

As calcium plays a major role in various cellular degenerative processes, we were interested in examining the role of Ca^{2+} in acrolein-mediated injury. We examined the extent of acrolein-mediated myelin damage in Ca^{2+} depleted media, supplemented with EGTA, a Ca^{2+} chelator (5 mM) and adjusted with an equivalent concentration of Mg^{2+} to maintain divalent cation levels. EGTA was applied 30 min before the onset of acrolein exposure (200 μM). We found that the depletion of Ca^{2+} significantly decreased acrolein-induced myelin retraction near the nodes of Ranvier (leading to nodal lengthening) in spinal cord ventral white matter. Specifically, the index of nodal length increased from a control level of 0.64 ± 0.07 ($n = 50$) to 1.87 ± 0.16 ($n = 79$) ($p < 0.01$) following acrolein incubation for 12 h (same data shown in Fig. 1). However, depletion of Ca^{2+} in the presence of acrolein prevented this change, maintaining the index of nodal length at 0.61 ± 0.07 ($n = 70$), which was significantly lower than acrolein only ($p < 0.01$) (Fig. 3a). The index of nodal length in Ca^{2+}-depletion group was not significantly different compared to control samples ($p > 0.05$). These data support the hypothesis that acrolein-induced nodal lengthening is Ca^{2+}-mediated, possibly mediated by the activation of a Ca^{2+}-dependent protease such as calpain. However, removal of Ca^{2+} did not alleviate myelin splitting in the

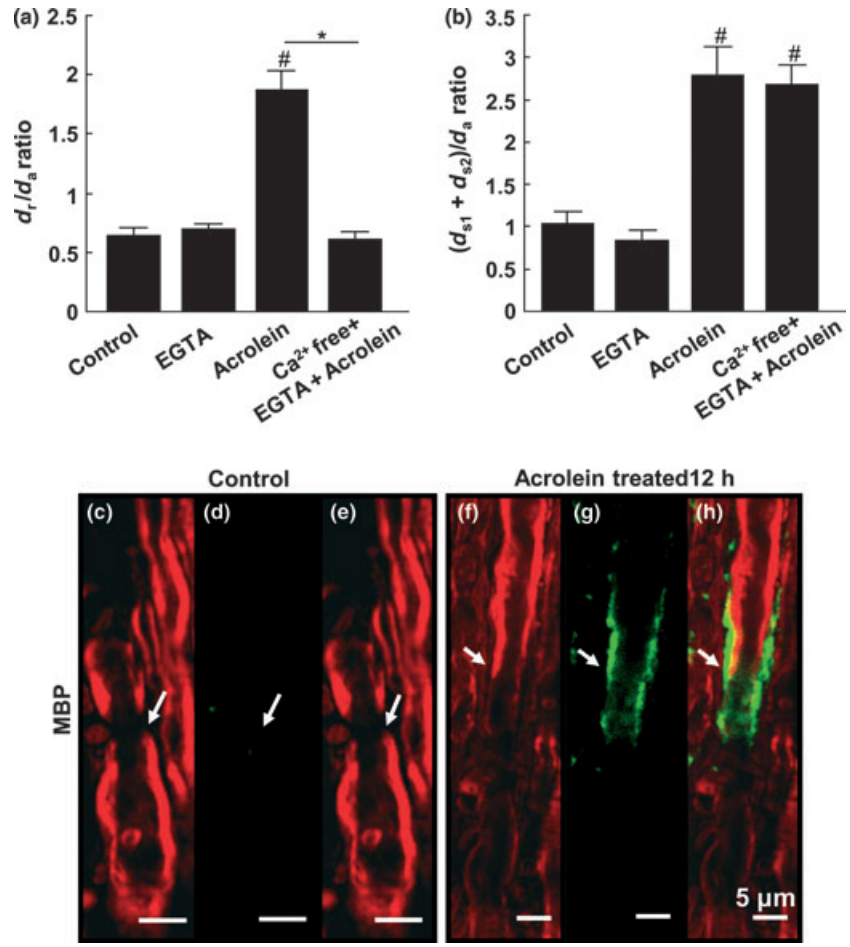

Fig. 3 Myelin retraction is Ca^{2+} dependent while myelin splitting is Ca^{2+} independent. (a) The bar graph for index of nodal length (d_t/d_a) shows that depletion of Ca^{2+} in extracellular space reduces nodal retraction induced by acrolein. Exposure to acrolein (200 μM) for 12 h significantly increases the index of node length from 0.64 ± 0.07 (n = 50) to 1.87 ± 0.16 (n = 79) ($p < 0.01$). In contrast, Ca^{2+} depletion significantly lowered the increase of index of nodal length induced by acrolein (0.61 ± 0.07, n = 70, $p < 0.01$ compared to acrolein only), which is not different compared to control ($p > 0.05$). (b) The bar graph for the index myelin splitting [$(d_{s1} + d_{s2})/d_a$] shows that depletion of Ca^{2+} in the extracellular space has little benefit on acrolein-induced nodal myelin splitting. Exposure to acrolein (200 μM) for 12 h significantly increases the index of paranodal myelin from 1.04 ± 0.14 (n = 50) to 2.79 ± 0.34 (n = 79, $p < 0.01$). In addition, Ca^{2+} depletion in the media (supplemented with EGTA) resulted in an index of paranodal myelin of 2.68 ± 0.23 (n = 70) which is not significantly different compared to those when Ca^{2+} was present ($p > 0.05$). #$p < 0.01$ compared to control. *$p < 0.05$. (c–h) CARS and immunofluorescence images of damaged myelin basic protein in response to acrolein application. (c–e) Tissue imaged by CARS (red) and by immunofluorescence stained for degenerated myelin basic protein (MBP) (green). Spinal cord tissue incubated with 200 μM acrolein for 12 h demonstrated degenerated MBP labeling (g) along the axon (f, h). In contrast, little MBP damage was detected without acrolein (d). Scale bar = 5 μm.

paranodal region. The index of paranodal myelin in the Ca^{2+}-depleted media that contains acrolein was not significantly different from that of acrolein alone (2.68 ± 0.23, n = 70, vs. 2.79 ± 0.34, n = 79, $p > 0.05$) (Fig. 3b). This suggests that acrolein-mediated myelin splitting is not Ca^{2+}-dependent.

Acrolein exposure damages myelin basic protein

Myelin basic protein (MBP) is one of the major components in myelin that could possibly be damaged by acrolein. To ascertain the existence and extent of acrolein-mediated MBP damage, we used immunofluorescence staining with specific antiserum raised against degraded MBP to examine the extent of MBP damage because of acrolein. Figure 3(c–h) shows representative confocal images of ventral white matter incubated for 12 h with either normal Krebs' solution (c–e) or 200 μM acrolein (f–h). Myelin sheaths were imaged by CARS (red), while immunofluorescence staining revealed degraded MBP (green). These two images were then superimposed (overlay) to reveal the location of degraded MBP in reference to myelin (Fig. 3e and h). No significant degraded MBP was visualized in the control group without acrolein treatment,

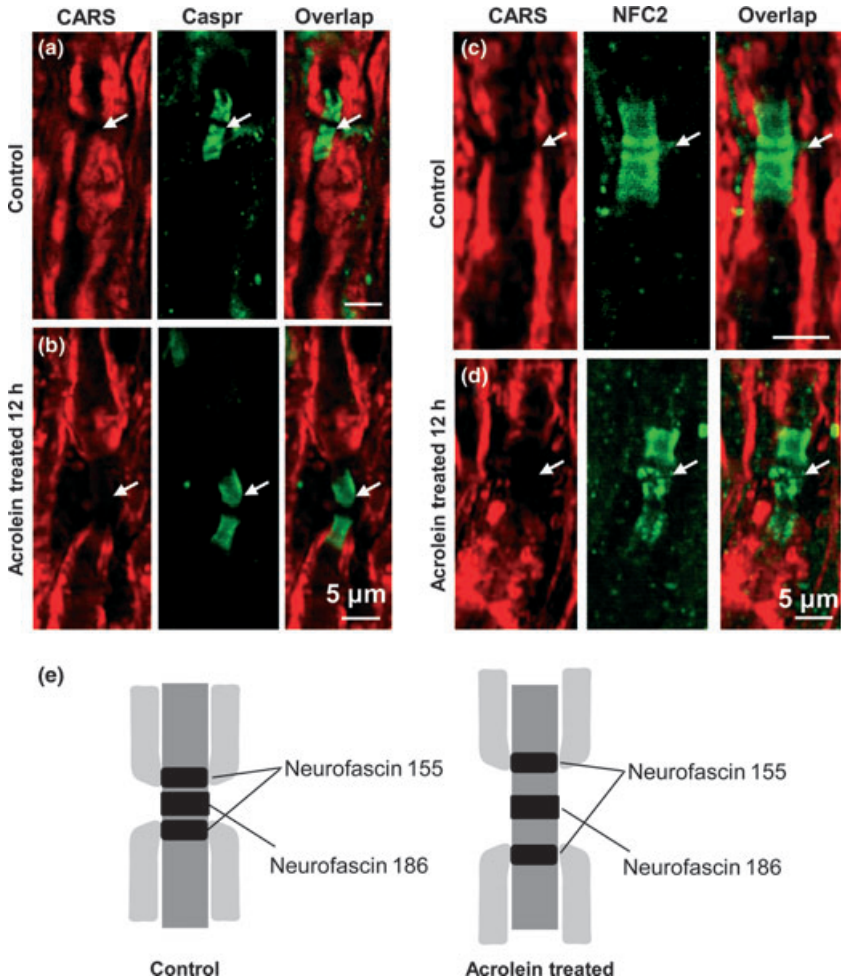

Fig. 4 Acrolein induced paranodal protein complex dissociation. For the left column, myelin sheath was identified by CARS (red) and Caspr protein was labeled by anti-Caspr and imaged with TPEF (green). Control tissue demonstrated the Caspr protein was covered by myelin sheath (a). Spinal cord tissue treated with 200 μM acrolein for 12 h showed noticeable elongation of node region as well as the exposure of Caspr protein (b). Arrows were pointing to node region. For the right column, anti-NFC2 was used to label neurofascin 186 and neurofascin 155 (green). Myelin sheath was imaged with CARS (red). (c) In control tissue, NCF2 labeling occupied both node and paranode region. (d) In tissue treated with acrolein, paranodal myelin was retracted. In addition, NCF2 labeling was separated into three segments: the middle component (likely neurofascin 186) remained at node of Ranvier while the lateral components (likely neurofascin 155) were retracted along with myelin sheath. (e) Scheme of NFC2 alteration after acrolein treatment as compared to control. Scale bar: 5 μm.

as displayed by very little green fluorescence (Fig. 3d). In contrast, incubation of spinal cord ventral white matter with acrolein at 200 μM for 12 h resulted in extensive staining of degraded MBP (Fig. 3g). Overlay images demonstrate colocalization (Fig. 3h) of degraded MBP (Fig. 3g) and myelin sheaths (Fig. 3f), confirming that the damage was indeed located along the myelin. The staining appeared to start from paranodal region and tended to diffuse into the internodal region (Fig. 3g and h).

Acrolein-induced paranodal protein complex dissociation and subsequent Kv 1.2 potassium channel exposure

Coherent anti-stokes Raman scattering imaging revealed splitting and retraction of the myelin sheath at nodes of Ranvier after acrolein treatment, indicating that the paranodal axo-glial complex may have been damaged. The paranodal axo-glial conjunction is formed by a protein complex composed of Caspr, Neurofasin155 (NF155) and contactin (Bhat *et al.* 2001; Bhat 2003; Poliak and Peles 2003). To investigate changes to the paranodal complex after acrolein treatment, we used immunofluorescence staining for Caspr and CARS images of myelin as a reference. From the control sample it was demonstrated that Caspr staining was localized at paranodal region and was aligned with and largely covered by the myelin sheath signal obtained from CARS (Fig. 4a). In contrast, when the spinal cord tissue was incubated with 200 μM acrolein for 12 h, the Caspr staining was dissociated from paranodal myelin sheath (Fig. 4b). In addition, we used anti-NFC2 to label both neurofascin 186 (node region) and neurofascin 155 (paranode region), and co-localized the NFC2 labeling with myelin sheath imaging from CARS (Fig. 4c and d).

From the NFC2 labeling, it appears that neurofascin 186 is normally localized to the node of Ranvier, consistent with its anchorage on the axonal membrane (Poliak and Peles 2003). This region is bordered on both ends by lateral components (likely neurofascin 155), supporting the notion that this protein stems from myelin which enwraps the axon (Poliak and Peles 2003). In acrolein treated samples, in addition to the paranodal myelin retraction we also demonstrated noticeable separation of three components in NFC2 labeling (Fig. 4d) compared to control sample (Fig. 4c). This suggests that neurofascin 186 remained in node of Ranvier region while neurofascin 155 retracted with the myelin sheath. This

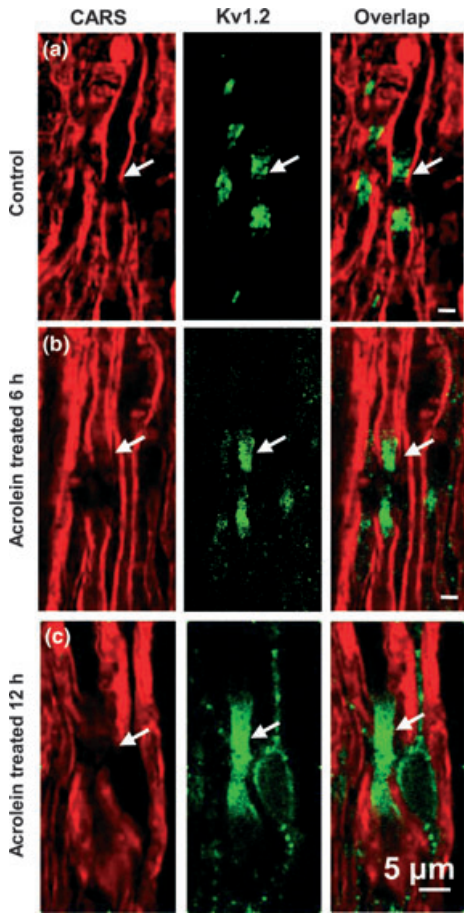

Fig. 5 Acrolein treatment exposed paranodal potassium channels. Myelin sheath was identified by CARS (red) and Kv 1.2 channels were labeled by anti-Kv 1.2 and imaged with TPEF (green). (a) Control image (without acrolein exposure) showed that Kv 1.2 (green, arrowhead) was well covered underneath myelin sheath at juxtaparanodal area. (b) Kv 1.2 (green) was partially exposed after exposure to acrolein at 200 μM for 6 h. (c) Redistribution of Kv 1.2 towards the node of Ranvier following incubation of acrolein at 200 μM for 12 h. Scale bar = 5 μm.

evidence further supports the assumption that acrolein induces paranodal protein complex dissociation.

Based on the histology of the node of Ranvier in myelinated axons, it is likely that the retraction of paranodal myelin and the lengthening of nodes of Ranvier could result in the exposure of potassium channels which are usually largely masked by myelin in the juxtaparanodal region in uninjured normal axons (Poliak and Peles 2003). We used immunofluorescent staining for voltage-gated potassium channels (VGPC) Kv 1.2 to determine their distribution in the uninjured cord (Fig. 5a). CARS images were employed to identify the location of myelin sheaths (red) while immunofluorescence signified potassium channels (green). As shown in Fig. 5(a), these potassium channels were covered by myelin in healthy axons. Intense staining of Kv 1.2 channels was observed to be restricted to the juxtaparanodal region, indicating high density of Kv channel aggregated and also restricted within this region. Please also note the complete absence of Kv 1.2 staining at the node of Ranvier (Fig. 5a). However, upon exposure to acrolein at 200 μM for 6 h, the Kv 1.2 staining was no longer completely covered by myelin, but partially exposed (Fig. 5b) while the node of Ranvier was lengthened (Fig. 5b). When exposed to acrolein at 200 μM for 12 h (Fig. 5c), it was clear that not only was the exposure of Kv 1.2 more severe, but the distribution of Kv 1.2 was more diffuse. Specifically, Kv 1.2 was observed throughout the node of Ranvier, and was no longer restricted to the paranodal and juxtaparanodal region. This phenomenon indicates that acrolein-mediated myelin damage resulted in the redistribution of potassium channels.

4-AP enhances action potential conduction in acrolein-treated spinal cord white matter axons

It is well known that one of the functional consequences of myelin damage is axonal conduction block (Waxman 1985; Shi and Blight 1997; Jensen and Shi 2003). This is thought to result from the exposure and activation of potassium channels as a result of myelin damage (in the case of current study, nodal lengthening), thus resulting in conduction block. It is also well known that potassium channel blockers, such as 4-AP, can enhance action potential conductance in axons with damaged myelin, but not in those with intact myelin (Shi and Blight 1997; Shi *et al.* 1997; Jensen and Shi 2003). Therefore, in order to gain electrophysiological evidence of myelin damage as a result of acrolein exposure, we investigated whether 4-AP enhances action potential conduction in acrolein-treated spinal cord white matter. As expected, we found that 4-AP was indeed capable of enhancing action potential conduction (Fig. 6) in white matter strips treated with acrolein. Specifically, electrophysiological examination of the CAPs using the double sucrose gap recording chamber showed a decline of the CAP amplitude to 91.7 ± 9.6% of pre-treatment values ($n = 6$) following 1–2 h exposure of acrolein at 100 μM, and to 54.3 ± 30.4% ($n = 4$) at 200 μM (Fig. 6c, both changes were significant compared to control, $p < 0.05$). 4-AP at 100 μM enhanced the CAP amplitude to 106.5 ± 1.3% in the group that pre-treated with 100 μM acrolein and to 106.3 ± 1.7% in the group that pre-treated with 200 μM acrolein treatment group (Fig. 6d, both changes were significant compared to pre-4-AP treatment, $p < 0.05$). Furthermore, acrolein treatment also decreased the duration of the CAP (measured at half-amplitude) which can be reversed upon 4-AP treatment (Fig. 6a and b). Specifically, there was a reduction in CAP duration to 90.1 ± 6.2% with 100 μM acrolein and to 86.5 ± 5.6% with 200 μM acrolein compared to control (Fig. 6e, both comparisons were significant, $p < 0.05$). 4-AP at 100 μM lengthened the duration of compound action

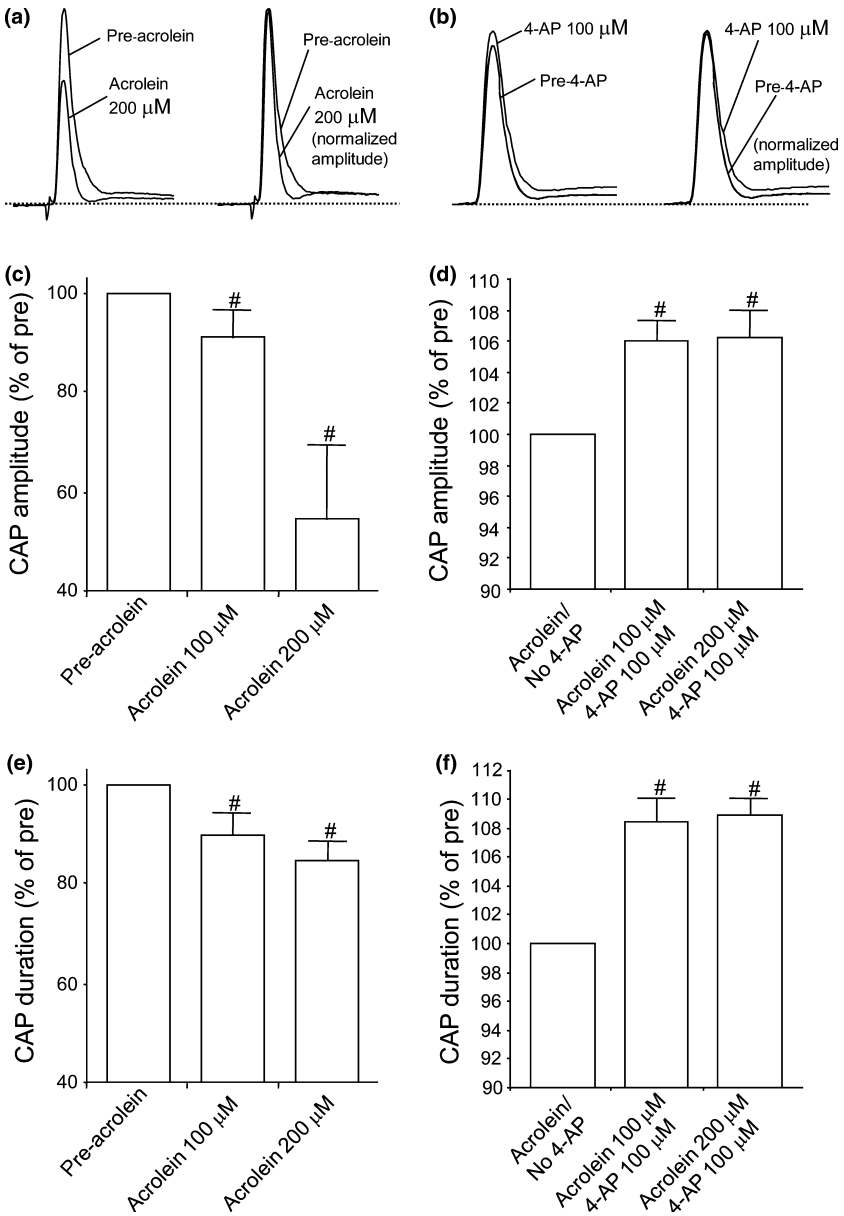

Fig. 6 CAP reduction during acrolein exposure and recovery after 4-AP treatment. (a) Representative CAP recordings before and after 200 μM acrolein treatment. It is demonstrated that acrolein treatment decreased CAP amplitude. When normalized the CAP amplitude to the same level, it is shown that the width of post-treatment CAP is narrower than the pre-treatment one. (b) Representative CAP recordings of spinal cord tissue in response to 100 μM 4-AP treatment after acrolein exposure. Besides increase in CAP amplitude, there is also a noticeable increase in CAP width. Histogram shows that acrolein at both 100 μM and 200 μM can produce significant decrease of the amplitude of CAP (#$p < 0.05$ compared to pre-acrolein, c), while 4-AP restores CAP amplitude in both groups ($p < 0.05$ compared to pre-4-AP, d). Furthermore, acrolein at both 100 μM and 200 μM significantly reduces the duration of CAP (#$p < 0.05$ compared to pre-acrolein, e), while 4-AP restores the CAP duration in both groups (#$p < 0.05$ compared to pre-4-AP, f).

potential to 108.5 ± 1.8% and 4-AP at 200 μM increased the duration to 109 ± 1.3% compared to pre-treatment (Fig. 6f, both comparisons were significant, $p < 0.05$). These observations suggest that acrolein-mediated myelin damages likely exposes potassium channels which can be effectively closed by treatment with 4-AP. Therefore, the functional analysis is consistent with histological observation that myelin is damaged at the paranodal region, leading to potassium channel exposure and action potential conduction block.

Discussion

Acrolein has been implicated as a potential toxin in previous studies of free radical mediated neuronal injuries (Esterbauer *et al.* 1991; Adams and Klaidman 1993; Kehrer and Biswal 2000; Luo and Shi 2004, 2005; Luo *et al.* 2005a; Hamann *et al.* 2008a,b). In the current study, we present evidence that acrolein is capable of damaging myelin. Considering its dual action in damaging both axons and myelin, acrolein may play a key role in the pathogenesis of MS and SCI where axonal and myelin injuries contribute to conduction block and partial or complete paralysis. Such hypothesis is consistent with a recent report that acrolein protein adducts levels were elevated significantly in the spinal cord of EAE mice, an animal model of MS where axonal damage and myelin disruption co-exist (Leung *et al.* 2011). To further support the pathological role of acrolein, anti-acrolein therapy significantly alleviated myelin damage, delayed the

onset, and reduced the severity of behavioral deficits associated with EAE (Leung *et al.* 2011).

The most conspicuous finding in this study is the structural alteration at the paranodal region, where we note a significant lengthening of the node of Ranvier (Fig. 1) and myelin splitting (Fig. 2). Specifically, morphometric analysis revealed acrolein increased the index of node length (d_r/d_a) up to 4-fold following 12 h of incubation (Fig. 1c). Concomitantly, the index of paranodal myelin [$(d_{s1} + d_{s2})/d_a$] near the node of Ranvier was more than doubled (Fig. 2c).

As this study involved no mechanical trauma, the most likely mechanism by which the node lengthening occurs is the retraction of the paranodal myelin towards the internodal region. We hypothesize that this pathology is mediated by the disruption of proteins at the axoglial paranodal junction. It has been reported previously that the axoglial paranodal junction is critical for maintaining the proper structure of the nodes of Ranvier (Poliak and Peles 2003). This axon-glial interaction is generated and maintained by an axoglial septate junction involving several proteins, such as Caspr (Einheber *et al.* 1997), contactin (Rios *et al.* 2000), Nfac 155 (Tao-Cheng and Rosenbluth 1983), protein 4.1 (Menegoz *et al.* 1997; Denisenko-Nehrbass *et al.* 2003), spectrin and actin (Kontrogianni-Konstantopoulos *et al.* 2001; Ogawa *et al.* 2006). In the current study, we observed that with 12 h acrolein treatment, the myelin sheath was detached from axonal Caspr (Fig. 4), which indicates the dissociation of paranodal protein complex. Interestingly, we also noted a separation of neurofascin 155 from neurofascin 186 (Fig. 4). This further confirms the destruction of axoglial septate junction.

In addition, decreasing calcium, a key coenzyme of various proteases such as calpain, significantly alleviated acrolein-mediated myelin retraction (Fig. 3a). It is known that calpain, a calcium dependent protease, can be activated as a result of acrolein incubation (Liu-Snyder *et al.* 2006b). Furthermore, both spectrin and protein 4.1 (components of axoglial septate junctions) are substrates of calpain it is likely that calpain activation could lead to interruption of the normal axoglial connection and structural abnormalities such as myelin retraction (Wang 2000; Goll *et al.* 2003).

We have found that paranodal myelin splitting, another form of myelin damage observed in this study, was not influenced by the depletion of extracellular calcium (Fig. 3). Based on degradation of MBP observed in the current study (Fig. 3f–h) at paranodal region, it is likely that acrolein reacts directly with myelin basic protein, which leads to delamination and myelin splitting (Omlin *et al.* 1982; Readhead *et al.* 1990; Boggs 2006).

It is well known that in the adult mammalian myelinated axons, the majority of the VGPC are located beneath the myelin and cluster in the juxtaparanodal region, while sodium channels aggregate at the node of Ranvier (Poliak and Peles 2003) (Fig. 5a). Using immunohistochemistry, we demonstrated exposure of potassium channels in the presence of acrolein (Fig. 5b). Furthermore, the finding that 4-AP, a potassium channel blocker, can partially restore conduction in this situation (Fig. 6) further supports the role of exposure of potassium channels in conduction failure (Sherratt *et al.* 1980; Shi and Blight 1997; Jensen and Shi 2003).

When the duration acrolein exposure was increased to 12 h, we noted an expansion of the VGPC distribution to the node of Ranvier (Fig. 5c). To our knowledge, there is no prior report that VGPC can be exposed and induced to expand across the node of Ranvier following acute incubation with an endogenous toxin such as acrolein. The mechanism of VGPC diffusion or redistribution is not likely to be explained by retraction of myelin alone, but could be linked to changes in the anchoring protein complex at the axoglial paranodal junction. It is suggested that the axoglial septate junction functions as a barrier that limits the movement of VGPC towards the nodes (Dupree *et al.* 1999; Poliak and Peles 2003). Therefore, removal of this barrier by damaging anchoring protein complexes could potentially lead to aberrant movement and redistribution of VGPC. In fact, in chronic multiple sclerosis, myelin damage is associated with abnormal distribution of Caspr (Wolswijk and Balesar 2003).

Although the focus of this paper was to specifically demonstrate acrolein-mediated myelin disruption, it is well established that acrolein can also cause severe neuronal membrane damage (Luo and Shi 2004). Therefore, it is more than likely that both acrolein-mediated axonal membrane damage and myelin disruption contribute to the functional failure in the current study. As the integrities of both myelin and axons are indispensible for neuronal function, therapies targeting only one of these deficits, membrane or myelin, are expected to only partially restore function. This may explain in part that the application of 4-AP which blocks potassium channel exposed because of myelin damage, can only partially restore CAP conductance (Fig. 6).

The concentrations of acrolein used to produce damage were between 200 and 500 μM. These values are consistent with concentrations employed in our previous models (1–500 μM) that produced various degrees of structural and functional damage in neurons (Shi *et al.* 2002; Luo and Shi 2004, 2005; Luo *et al.* 2005a; Liu-Snyder *et al.* 2006a,b; Hamann *et al.* 2008b). Although the exact concentration of acrolein in trauma or neurodegenerative diseases has not been determined, we believe acrolein at μM-mM levels is likely found in human and animal tissues under diseases states. For example, the concentration of acrolein is reported to reach 80 μM in the fluid of respiratory tract of smokers (Nardini *et al.* 2002) and 180 μM in the plasma of patients with renal failure (Sakata *et al.* 2003). The concentration of acrolein in the brain of Alzheimer's disease patients has been found to increase 4-fold to a range of 2.5–5 nmol/mg protein (Lovell *et al.* 2001). We previously estimated that 100–

500 μM acrolein corresponds to 1.0–5.2 nmol/mg protein in spinal cord (Hamann *et al.* 2008b), which is similar to the concentrations in Alzheimer's disease brains, and thus may be within the scope of MS and SCI victims as well.

Another factor in the pathophysiology of acrolein-mediated toxicity is the duration. Because of the limitations of our *ex vivo* experimentation, the longest incubation time for acrolein was 12 h. However, acrolein levels are likely elevated significantly longer *in vivo*. Luo *et al.* (2005b) reported that acrolein production is increased for at least 7 days following spinal cord compression. In chronic neurodegenerative diseases where the course of the ailment progresses for years, acrolein concentrations are likely elevated for much longer periods. Additionally, other secondary outcomes of injury, such as ischemia (Sandler and Tator 1976; Hall and Wolf 1987; White *et al.* 2000) can significantly exacerbate acrolein mediated neuronal insult (Peasley and Shi 2003). Thus, the threshold of acrolein that can inflict significant damage *in vivo* may actually be lower than the values used in this study (100–500 μM) because of exposure time and potential coupling effects *in vivo*. Taken together, we conclude that acrolein may play a critical role in mediating neuronal and myelin damage and represents a novel target in treating neuronal degenerative diseases and trauma.

Acknowledgements

This research was supported by the NIH (1R01EB007243) and the State of Indiana. Special thanks to Gary Leung for isolation of spinal cord white matter strips from guinea pigs. We also thank Todd Rickett and Dr. Jianming Li for his critical reading for this manuscript.

References

Adams Jr J. D. and Klaidman L. K. (1993) Acrolein-induced oxygen radical formation. *Free Radic. Biol. Med.* **15**, 187–193.

Bhat M. A. (2003) Molecular organiazation of axo-glial junctions. *Curr. Opin. Neurobiol.* **13**, 552–559.

Bhat M. A., Rios J. C., Lu Y. *et al.* (2001) Axon-glia interactions and the domain organization of myelinated axons requires neurexin IV/Caspr/Paranodin. *Neuron* **30**, 369–383.

Blight A. R. (1985) Delayed demyelination and macrophage invasion: a candidate for secondary cell damage in spinal cord injury. *Cent. Nerv. Syst. Trauma* **2**, 299–315.

Boggs J. M. (2006) Myelin basic protein: a multifunctional protein. *Cell. Mol. Life Sci.* **63**, 1945–1961.

Calabrese V., Bella R., Testa D., Spadaro F., Scrofani A., Rizza V. and Pennisi G. (1998) Increased cerebrospinal fluid and plasma levels of ultraweak chemiluminescence are associated with changes in the thiol pool and lipid-soluble fluorescence in multiple sclerosis: the pathogenic role of oxidative stress. *Drugs Exp. Clin. Res.* **24**, 125–131.

Compston A. and Coles A. (2008) Multiple sclerosis. *Lancet* **372**, 1502–1517.

Denisenko-Nehrbass N., Oguievetskaia K., Goutebroze L., Galvez T., Yamakawa H., Ohara O., Carnaud M. and Girault J. A. (2003) Protein 4.1B associates with both Caspr/paranodin and Caspr2 at paranodes and juxtaparanodes of myelinated fibres. *Eur. J. Neurosci.* **17**, 411–416.

Dupree J. L., Girault J. A. and Popko B. (1999) Axo-glial interactions regulate the localization of axonal paranodal proteins. *J. Cell Biol.* **147**, 1145–1152.

Einheber S., Zanazzi G., Ching W., Scherer S., Milner T. A., Peles E. and Salzer J. L. (1997) The axonal membrane protein Caspr, a homologue of neurexin IV, is a component of the septate-like paranodal junctions that assemble during myelination. *J. Cell Biol.* **139**, 1495–1506.

Esterbauer H., Schaur R. J. and Zollner H. (1991) Chemistry and biochemistry of 4-hydroxynonenal, malonaldehyde and related aldehydes. *Free Radic. Biol. Med.* **11**, 81–128.

Fu Y., Wang H., Huff T. B., Shi R. and Cheng J. X. (2007) Coherent anti-Stokes Raman scattering imaging of myelin degradation reveals a calcium-dependent pathway in lyso-PtdCho-induced demyelination. *J. Neurosci. Res.* **85**, 2870–2881.

Ghilarducci D. P. and Tjeerdema R. S. (1995) Fate and effects of acrolein. *Rev. Environ. Contam. Toxicol.* **144**, 95–146.

Gold R., Linington C. and Lassmann H. (2006) Understanding pathogenesis and therapy of multiple sclerosis via animal models: 70 years of merits and culprits in experimental autoimmune encephalomyelitis research. *Brain* **129**, 1953–1971.

Goll D. E., Thompson V. F., Li H., Wei W. and Cong J. (2003) The calpain system. *Physiol. Rev.* **83**, 731–801.

Gonsette R. E. (2008) Neurodegeneration in multiple sclerosis: the role of oxidative stress and excitotoxicity. *J. Neurol. Sci.* **274**, 48–53.

Hall E. D. (1989) Free radicals and CNS injury. *Crit. Care Clin.* **5**, 793–805.

Hall E. D. and Wolf D. L. (1987) Post-traumatic spinal cord ischemia: relationship to injury severity and physiological parameters. *Cent. Nerv. Syst. Trauma* **4**, 15–25.

Hamann K., Durkes A., Ouyang H., Uchida K., Pond A. and Shi R. (2008a) Critical role of acrolein in secondary injury following ex vivo spinal cord trauma. *J. Neurochem.* **107**, 712–721.

Hamann K., Nehrt G., Ouyang H., Duerstock B. and Shi R. (2008b) Hydralazine inhibits compression and acrolein-mediated injuries in ex vivo spinal cord. *J. Neurochem.* **104**, 708–718.

Jana A. and Pahan K. (2007) Oxidative stress kills human primary oligodendrocytes via neutral sphingomyelinase: implications for multiple sclerosis. *J. Neuroimmune. Pharmacol.* **2**, 184–193.

Jensen J. M. and Shi R. (2003) Effects of 4-aminopyridine on stretched mammalian spinal cord: the role of potassium channels in axonal conduction. *J. Neurophysiol.* **90**, 2334–2340.

Kehrer J. P. and Biswal S. S. (2000) The molecular effects of acrolein. *Toxicol. Sci.* **57**, 6–15.

Koch M., Ramsaransing G. S., Arutjunyan A. V., Stepanov M., Teelken A., Heersema D. J. and De Keyser J. (2006) Oxidative stress in serum and peripheral blood leukocytes in patients with different disease courses of multiple sclerosis. *J. Neurol.* **253**, 483–487.

Kontrogianni-Konstantopoulos A., Frye C. S., Benz Jr E. J. and Huang S. C. (2001) The prototypical 4.1R-10-kDa domain and the 4.1g-10-kDa paralog mediate fodrin-actin complex formation. *J. Biol. Chem.* **276**, 20679–20687.

Leung G., Sun W., Zheng L., Brookes S., Tully M. and Shi R. (2011) Anti-acrolein treatment improves behavioral outcome and alleviates myelin damage in experimental autoimmune encephalomyelitis mouse. *Neuroscience* **26**, 150–155.

LeVine S. M. (1992) The role of reactive oxygen species in the pathogenesis of multiple sclerosis. *Med. Hypotheses* **39**, 271–274.

Li S. and Stys P. K. (2000) Mechanisms of ionotropic glutamate receptor-mediated excitotoxicity in isolated spinal cord white matter. *J. Neurosci.* **20**, 1190–1198.

Liu-Snyder P., Borgens R. B. and Shi R. (2006a) Hydralazine rescues PC12 cells from acrolein-mediated death. *J. Neurosci. Res.* **84**, 219–227.

Liu-Snyder P., McNally H., Shi R. and Borgens R. B. (2006b) Acrolein-mediated mechanisms of neuronal death. *J. Neurosci. Res.* **84**, 209–218.

Lovell M. A., Xie C. and Markesbery W. R. (2000) Acrolein, a product of lipid peroxidation, inhibits glucose and glutamate uptake in primary neuronal cultures. *Free Radic. Biol. Med.* **29**, 714–720.

Lovell M. A., Xie C. and Markesbery W. R. (2001) Acrolein is increased in Alzheimer's disease brain and is toxic to primary hippocampal cultures. *Neurobio. Aging* **22**, 187–194.

Luo J. and Shi R. (2004) Acrolein induces axolemmal disruption, oxidative stress, and mitochondrial impairment in spinal cord tissue. *Neurochem. Int.* **44**, 475–486.

Luo J. and Shi R. (2005) Acrolein induces oxidative stress in brain mitochondria. *Neurochem. Int.* **46**, 243–252.

Luo J., Robinson J. P. and Shi R. (2005a) Acrolein-induced cell death in PC12 cells: role of mitochondria-mediated oxidative stress. *Neurochem. Int.* **47**, 449–457.

Luo J., Uchida K. and Shi R. (2005b) Accumulation of acrolein-protein adducts after traumatic spinal cord injury. *Neurochem. Res.* **30**, 291–295.

Menegoz M., Gaspar P., Le Bert M., Galvez T., Burgaya F., Palfrey C., Ezan P., Arnos F. and Girault J. A. (1997) Paranodin, a glycoprotein of neuronal paranodal membranes. *Neuron* **19**, 319–331.

Nardini M., Finkelstein E. I., Reddy S., Valacchi G., Traber M., Cross C. E. and Van der Vliet A. (2002) Acrolein-induced cytotoxicity in cultured human bronchial epithelial cells. Modulation by alpha-tocopherol and ascorbic acid. *Toxicology* **170**, 173–185.

Ogawa Y., Schafer D. P., Horresh I., Bar V., Hales K., Yang Y., Susuki K., Peles E., Stankewich M. C. and Rasband M. N. (2006) Spectrins and ankyrinB constitute a specialized paranodal cytoskeleton. *J. Neurosci.* **26**, 5230–5239.

Omlin F. X., Webster H. D., Palkovits C. G. and Cohen S. R. (1982) Immunocytochemical localization of basic protein in major dense line regions of central and peripheral myelin. *J. Cell Biol.* **95**, 242–248.

Peasley M. A. and Shi R. (2003) Ischemic insult exacerbates acrolein-induced conduction loss and axonal membrane disruption in guinea pig spinal cord white matter. *J. Neurol. Sci.* **216**, 23–32.

Poliak S. and Peles E. (2003) The local differentiation of myelinated axons at nodes of Ranvier. *Nat. Rev. Neurosci.* **4**, 968–980.

Povlishock J. T. and Kontos H. A. (1992) The role of oxygen radicals in the pathobiology of traumatic brain injury. *Hum. Cell* **5**, 345–353.

Readhead C., Takasashi N., Shine H. D., Saavedra R., Sidman R. and Hood L. (1990) Role of myelin basic protein in the formation of central nervous system myelin. *Ann. N Y Acad. Sci.* **605**, 280–285.

Rios J. C., Melendez-Vasquez C. V., Einheber S., Lustig M., Grumet M., Hemperly J., Peles E. and Salzer J. L. (2000) Contactin-associated protein (Caspr) and contactin form a complex that is targeted to the paranodal junctions during myelination. *J. Neurosci.* **20**, 8354–8364.

Sakata K., Kashiwagi K., Sharmin S., Ueda S., Irie Y., Murotani N. and Igarashi K. (2003) Increase in putrescine, amine oxidase, and acrolein in plasma of renal failure patients. *Biochem. Biophys. Res. Commun.* **305**, 143–149.

Sandler A. N. and Tator C. H. (1976) Review of the effect of spinal cord trauma on the vessels and blood flow in the spinal cord. *J. Neurosurg.* **45**, 638–646.

Sasaki M., Black J. A., Lankford K. L., Tokuno H. A., Waxman S. G. and Kocsis J. D. (2006) Molecular reconstruction of nodes of Ranvier after remyelination by transplanted olfactory ensheathing cells in the demyelinated spinal cord. *J. Neurosci.* **26**, 1803–1812.

Sherratt R. M., Bostock H. and Sears T. A. (1980) Effects of 4-aminopyridine on normal and demyelinated mammalian nerve fibers. *Nature* **283**, 570–572.

Shi R. and Blight A. R. (1996) Compression injury of mammalian spinal cord in vitro and the dynamics of action potential conduction failure. *J. Neurophysiol.* **76**, 1572–1580.

Shi R. and Blight A. R. (1997) Differential effects of low and high concentrations of 4-aminopyridine on axonal conduction in normal and injured spinal cord. *Neuroscience* **77**, 553–562.

Shi R. and Borgens R. B. (1999) Acute repair of crushed guinea pig spinal cord by polyethylene glycol. *J. Neurophysiol.* **81**, 2406–2414.

Shi R. and Whitebone J. (2006) Conduction deficits and membrane disruption of spinal cord axons as a function of magnitude and rate of strain. *J. Neurophysiol.* **95**, 3384–3390.

Shi R., Kelly T. M. and Blight A. R. (1997) Conduction block in acute and chronic spinal cord injury: different dose-response characteristics for reversal by 4-Aminopyridine. *Exp. Neurol.* **148**, 495–501.

Shi R., Luo J. and Peasley M. A. (2002) Acrolein inflicts axonal membrane disruption and conduction loss in isolated guinea pig spinal cord. *Neuroscience* **115**, 337–340.

Smith K. J., Kapoor R. and Felts P. A. (1999) Demyelination: the role of reactive oxygen and nitrogen species. *Brain Pathol.* **9**, 69–92.

Tao-Cheng J. H. and Rosenbluth J. (1983) Axolemmal differentiation in myelinated fibers of rat peripheral nerves. *Brain Res.* **285**, 251–263.

Wang K. K. (2000) Calpain and caspase: can you tell the difference? *Trends Neurosci.* **23**, 20–26.

Wang H., Fu Y., Zickmund P., Shi R. and Cheng J. X. (2005) Coherent anti-stokes Raman scattering imaging of axonal myelin in live spinal tissues. *Biophys. J.* **89**, 581–591.

Waxman S. G. (1985). Structure and function of the myelinated fiber, in *Handbook of Clinical Neurology*, Vol. 3 (**47**): Demyelinating Diseases (Koetsier J. C., ed.), pp. 1–28. Elsevier, Amsterdam.

White B. C., Sullivan J. M., DeGracia D. J., O'Neil B. J., Neumar R. W., Grossman L. I., Rafols J. A. and Krause G. S. (2000) Brain ischemia and reperfusion: molecular mechanisms of neuronal injury. *J. Neurol. Sci.* **179**, 1–33.

Wolswijk G. and Balesar R. (2003) Changes in the expression and localization of the paranodal protein Caspr on axons in chronic multiple sclerosis. *Brain* **126**, 1638–1649.